Solvent-free production of nanoscale zero-valent iron (nZVI) with precision milling

Shaolin Li, Weile Yan and Wei-xian Zhang*

Received 23rd April 2009, Accepted 10th June 2009
First published as an Advance Article on the web 24th July 2009
DOI: 10.1039/b913056j

Despite its effectiveness in degrading a wide array of environmental contaminants and superior physical characteristics for subsurface delivery, large-scale applications of nanoscale zero-valent iron (nZVI) for environmental remediation have been inhibited by the high costs associated with its conventional production technologies. In this contribution, an environmentally-benign and cost-effective production method of nZVI is demonstrated using a precision milling system. Unlike conventional methods such as chemical synthesis and vapor phase condensation, which typically involve toxic chemicals, sophisticated equipment and extensive labor, the precision milling method relies solely on the mechanical impact forces generated by stainless steel beads in a high-speed rotary chamber to break down the micro iron particles. The system uses no toxic solvents, is completely scalable to large-scale manufacturing. Scanning electron microscope (SEM) and BET surface area analysis independently verify that, after 8 hours of milling, the feed micro iron was effectively reduced to particles with sizes below 50 nm. The surface chemistry and crystal composition of the milled iron were characterized with high-resolution X-ray photoelectron spectroscopy (HR-XPS) and X-ray diffraction (XRD). Reactivity of the milled nZVI was probed through reactions with water and seven model chlorinated aliphatic compounds. The results demonstrate the milled nZVI (8 hour) is more reactive for contaminant degradation than the nZVI synthesized by the widely-adopted borohydride reduction method. The ball milling method thus stands as a promising green process for large-scale nZVI production and enhances the prospect of the nZVI technology for large-scale environmental remediation.

Introduction

Zero-valent iron (ZVI) has long been used as a cost-effective reductant for the treatment of a wide array of environmental contaminants including halogenated organic compounds, nitro aromatic compounds, arsenic, nitrate, azo dyes and heavy metal ions.[1–7] Moreover, ZVI is regarded as a green material because of the large amount of iron available as recycled materials, its benign toxicological properties, and its ability to completely degrade some contaminants with minimal secondary contamination. Conventional ZVI technology is typically applied in the form of permeable reactive barriers (PRBs) for groundwater remediation or in packed bed filters for enhanced wastewater treatment.[8,9] The extension of ZVI technology to nanoscale dimension has created a new class of ZVI material with significantly enhanced reactivity owing to its diminutive size and large surface area. Because of the small physical dimensions, nanoscale zero-valent iron (nZVI) is amenable to direct injection into contaminated groundwater and soils, and effective subsurface transport can be achieved with the use of appropriate dispersing agents.[10–12]

Department of Civil and Environmental Engineering, Lehigh University, Bethlehem, Pennsylvania, 18015, USA. E-mail: wez3@lehigh.edu; Tel: 610-758-5318

The classical method used in the nZVI synthesis is the reduction of ferrous or ferric ion by borohydride in an aqueous solution,[11–16]

$$2\,Fe(H_2O)_6^{3+} + 6\,BH_4^- + 6\,H_2O \rightarrow 2\,Fe^0(s) + 6\,B(OH)_3 + 21\,H_2(g) \quad (1)$$

This method, conducted under ambient temperature and pressure, can be routinely performed in common wet chemistry labs. The procedures have been well documented and widely adopted by laboratories worldwide. In spite of this, the wet chemistry approach is very expensive (>$200 per kg nZVI) due to the high cost of sodium borohydride (~$25 per lb) and the labor required. Aside from cost reasons, the approach suffers serious drawbacks for large-scale manufacturing because it requires additional processes for the separation and removal of byproducts such as borate. In addition, the wet chemistry method produces a large volume of wastewater.

Two general approaches exist for nanoparticle manufacturing: bottom-up and top-down methods (Fig. 1). Bottom-up approach entails piecing together individual atoms or molecules to form nanosized structures. For example, gas condensation produces iron nanoparticles by condensing atomic iron vapor in vacuum or under inert gas atmosphere.[17,18] Inevitably, generating metal vapor consumes a large amount of energy for heating and cooling, and vapor condensation and collection require highly restricted conditions, both of which necessitate complex and

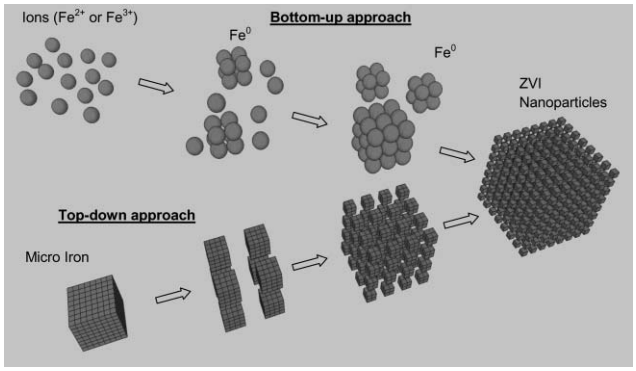

Fig. 1 Conceptual models of bottom-up and top-down approaches for nanoparticle preparations.

expensive working environment and equipment. As a result, gas condensation has largely been limited to lab-scale research and development. The yield is low, typically on the order of grams of nanoparticles per batch.[18]

In recent years, many alternative methods have been reported, among which some followed the conventional chemical synthesis routes *via* ferric or ferrous ion reduction by strong reductants. Compared to gas condensation, chemical reduction offers simplicity in operation (*e.g.*, under ambient pressure and temperature) and convenience in quality control.[16,19–26] However, chemical reactions often consume expensive and sometimes toxic reagents, and produce not only nZVI but also byproducts such as $B(OH)_3$. For example, thermal decomposition of iron pentacarbonyl ($Fe(CO)_5$) generates small and uniform-sized nZVI (~5 nm in diameter),[19] but iron pentacarbonyl is a highly toxic and unstable reagent and thus this approach raises critical safety concerns.

The top-down approach, on the other hand, is the process of breaking large bulk materials to smaller particles. Size reduction is usually achieved by mechanical means, with ball milling being perhaps the most common technique. In contrast to the complex procedures involved in the chemical synthesis, the principle of ball milling is straightforward: it strikes and breaks the micro- or millimetre scale starting materials with much larger and heavier milling media (balls or beads). No hazardous chemical is needed for milling. Furthermore, scale-up of ball milling has been widely deployed in many fields, especially in ultrafine powder, metal alloys, paints and pigments manufacturing.[27–29] Nevertheless, mechanical milling has rarely been applied to nanoparticle production so far, partly due to the limitation of the conventional equipment to achieve size reduction down to the nanometre scale. In addition, mechanical forces during milling introduce considerable dislocations, vacancies and strain to the products.[28] Consequently, the products are highly deformed with irregular shapes and contain a high level of defects that make them unsuitable for electronic and catalyst applications.[27,28]

Research presented in this contribution demonstrates that precision ball milling, with micro iron powder as the starting material, can produce nanoscale ZVI particles with major physicochemical properties consistent with, in some cases superior to, those of the chemically synthesized nZVI as confirmed by various characterization techniques. Specifically, Brunauer–Emmett–Teller (BET) surface area analysis was used to provide a quick assessment on the size reduction. Size and morphological changes were observed using a scanning electron microscope (SEM). High-resolution X-ray photoelectron spectroscopy (HR-XPS) and X-ray diffraction (XRD) were applied to determine the surface and the structure compositions. Solution chemistry in the forms of pH and E_h changes were recorded to assess the aqueous reactivity of the produced nanoparticles. Reactivity towards a group of common chlorinated aliphatic hydrocarbons was measured and compared with that of the chemically synthesized nZVI.

Experimental

Materials

Microscale zero-valent iron (BASF, iron content >99%, d_{50} = 2 μm) was used as the feed material. The following seven chlorinated aliphatic hydrocarbons were used as model contaminants to assess the iron reactivity: 1,1-dichloroethane (1,1-DCA, $CHCl_2CH_3$, Aldrich, >99.8%), 1,1,1-trichloroethane (1,1,1-TCA, CCl_3CH_3, Aldrich, ≥99.5%), tetrachloromethane (CT, CCl_4, Aldrich, ≥99.5%), 1,2-dichloroethane (1,2-DCA, CH_2ClCH_2Cl, Aldrich, >99.8%), trichloroethene (TCE, C_2HCl_3, Aldrich, ≥99.5%), tetrachloroethene (PCE, C_2Cl_4, Aldrich, 99.9%) and 1,1,2,2-tetrachloroethane (1,1,2,2-TeCA, $CHCl_2CHCl_2$, Aldrich, 99.8%). Ferric chloride anhydrous ($FeCl_3$) and sodium borohydride ($NaBH_4$, 98%) were purchased from Alfa Aesar and Finnish Chemical, Finland, respectively. High purity nitrogen gas was produced by Airgas, PA. All chemicals were used as received.

Ball milling for nanoparticle production

A laboratory-use ball mill (Labstar®) was purchased from Netzsch (Exton, PA, USA). As illustrated in Fig. 2, the entire setup includes 2 sub-systems: (1) the milling system consisting of a motor, a grinding chamber, an agitator and beads, and (2) a particle circulation and cooling system containing a pump and a holding tank to control the temperature of the iron suspension in

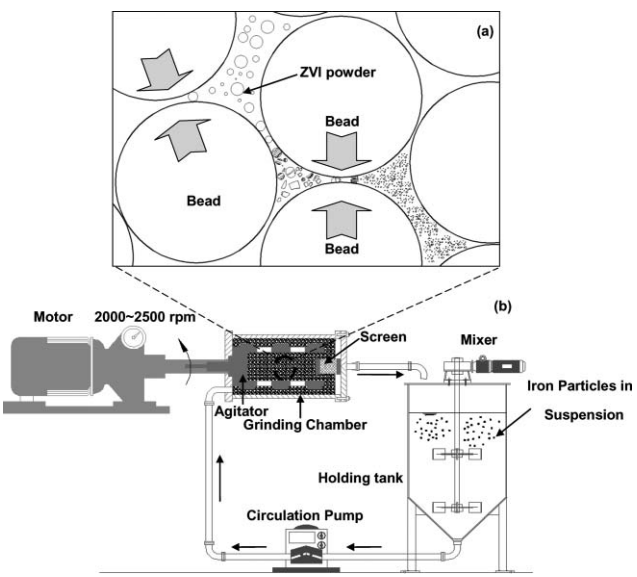

Fig. 2 (a) Illustration of collisions during milling and particle attrition. (b) Schematic drawing of a laboratory-scale milling system.

the tank and inside the mill. In a typical milling cycle, 1–2 kg of iron can be processed per batch. The settings used and the results achieved (*e.g.*, power input, milling time, and product yield) on this mill are linearly scalable for large-scale production-sized mills which can process over 1000 kg of iron each batch.[30]

The motor, through a shaft connected to the agitator, provides the milling power (P_{max} = 2.6 kW). The agitator, a hollow cylinder with arms and open slots, fits centrically in the stationary grinding chamber that has a capacity of approximately 700 ml. 450 ml (apparent volume) of steel beads (dia. 250 μm) is loaded into the chamber as the milling medium. During milling, the motor drives the agitator at a designated rotating speed (2000–2500 rpm) to stir up the milling medium (beads). Iron particles are smashed by the moving beads, and the impact energy fractures the material into smaller pieces. A stainless steel cylinder screen with laser-cut slots fits in at the open end of the agitator, which functions as a filter to retain the milling beads but allowing the processed iron material to pass through and go into the holding tank. From the holding tank the iron particles are recycled back to the milling system by the circulation pump. The milling procedure used here begins with mixing 1000 grams of the feed particles in the holding tank for 30 minutes before the circulation pump and the motor are turned on. The energy input to the system can be adjusted by the pump speed and the rotating speed of the agitator. Iron samples can be collected at the outlet of the grinding chamber to assess the size reduction.

Surface area, size and composition characterization

SEM imaging was performed using a field-emission SEM (Hitachi S-4300) operating at 5.0 kV. Specific surface area of the iron particles was measured using a Micrometrics Flowsorb 2305 following the classic Brunauer–Emmett–Teller (BET) method. Dried samples were first degassed at 170 °C for 40 minutes. Adsorption of pure nitrogen by iron sample was done in a sample tube at prescribed conditions followed by desorption of nitrogen as the temperature ramps up to room conditions. The amounts of nitrogen adsorbed and desorbed by the iron particles were measured and were used to calculate the total surface area and the mass-normalized specific surface area.

The as-prepared samples were analyzed with high-resolution X-ray photoelectron spectroscopy (HR-XPS) and X-ray diffraction (XRD) to determine their surface chemistry and crystal phase compositions. HR-XPS was carried out with a Scienta ESCA-300 instrument equipped with an Al rotating anode operated at 3.8 kW to produce 1486.6 eV Kα X-rays, seven crystals for X-ray monochromatization and a 300 mm mean radius hemispherical electron energy analyzer. A Rigaku diffractometer (Rigaku, Japan) with Cu Kα radiation generated at 40 kV and 30 mA was used to perform XRD analysis. Iron samples were scanned from 2-theta 10° to 80° with a stepping size of 0.1° and a scanning rate of 30 s per step. Details of the methods have been published.[31]

Solution pH and ORP measurements

Solution pH and oxidation-reduction potential (ORP) profiles of the produced nZVI were recorded in a four-neck 500 ml flask with three customized ports for pH, redox potential electrodes and nitrogen purging, respectively. Deionized (DI) water was deoxygenated by purging high-purity nitrogen gas for 30 min prior to the addition of nZVI. During the experiment, nitrogen gas was continuously introduced to the headspace to minimize oxygen intrusion. An adjustable speed mixer set at 600 rpm mixed the iron-water suspension during the experiment. A combination pH probe and an Ag/AgCl reference electrode (Cole-Parmer) were used with two Thermo Orion pH/ORP meters for solution pH and ORP monitoring, respectively. The redox potential readings (mV) obtained were calibrated to the standard hydrogen electrode potential (SHE) by adding +202 mV at 25 °C.

Chemical reactivity assessment

A series of batch experiments were conducted to examine the reactions of nZVI with chlorinated contaminants. Solutions of the seven model chlorinated aliphatic hydrocarbons (1,1-DCA, 1,1,1-TCA, CT, 1,2-DCA, TCE, PCE and 1,1,2,2-TeCA) were mixed with the milled iron particles in 125 ml serum bottles sealed with PTFE-lined crimp caps. Control experiments without nZVI were conducted in parallel. The batch reactors were agitated on a shaker at 300 rpm at room temperature. Concentrations of the chlorinated compounds were measured with a Shimadzu gas chromatograph/mass spectrometer (GC/MS, QP-5000) following the procedure described in ref. 32.

Results and discussion

Size characterization with SEM

The progressive size reduction was chronicled by SEM and BET surface area measurements of iron samples taken at various stages of the milling process. SEM imaging offers visual confirmation of the particle size, shape, morphology and the state of aggregation, while BET surface area measurement provides a simple and quantitative means to gauge the size change.

SEM images of the feed iron material and the finished product after 8 hours of milling are presented in Fig. 3. As shown in Fig. 3a and b, feed iron consists of spherical particles in the size range of 1–5 microns. Samples from different batches of the feed iron show comparable sizes. The results are consistent with the information provided by the supplier, which suggests a d_{50} of 2 μm.

Fig. 3c and d show the images of iron particles after 8 hours of continuous milling. Note that the scale bars in Fig. 3c and d represent 200 nm. The reduction in the particle sizes before and after milling is evident. Particle sizes observed after milling are mostly in the range of 10–50 nm with a fairly narrow size distribution. By direct visual inspection, the milled nZVI appears to be slightly smaller than those iron nanoparticles produced by the sodium borohydride reduction method in our lab, the representative diameter of which is 60 nm,[31] and those by the H_2 reduction method reported elsewhere, of which the suggested diameter is 70 nm.[15] Close-up observation of these images reveals that the particles made by milling exhibit irregular flaky shapes, in contrast to the smooth round-shaped nZVI produced by the chemical reduction method.[12,15] Previous investigations on ball milling suggest that particles are heavily impacted by the colliding beads and experience great

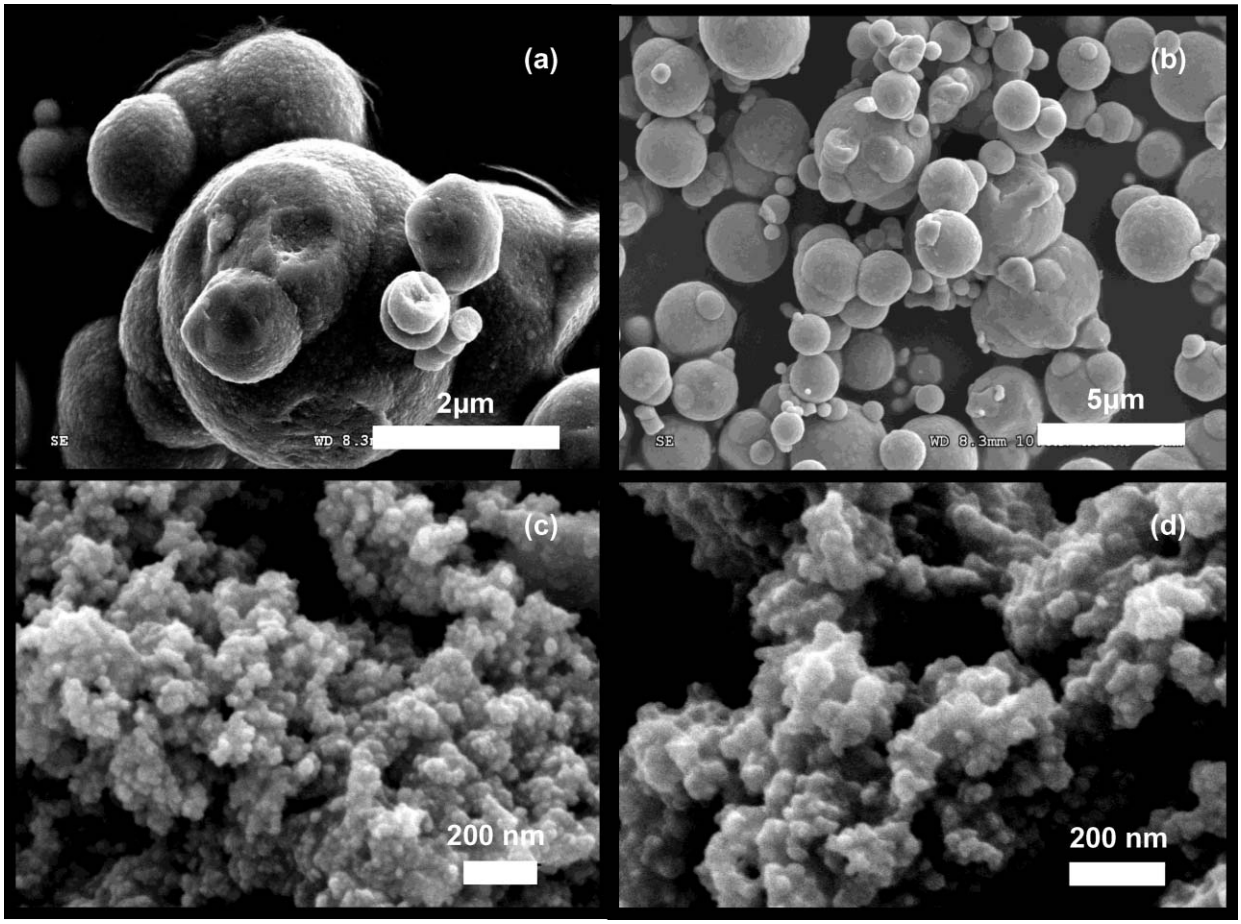

Fig. 3 SEM images of feed micro iron (a and b) and iron milled for 8 hours (c and d).

deformation and fracturing throughout the milling process, thus the final products are irregularly shaped with considerable internal and surface defects.[27] Meanwhile, extensive agglomeration can also be observed in Fig. 3c and d, giving rise to loose clusters of micron-scale dimensions. Previous works suggest that the agglomeration of nZVI can be effectively mitigated through the use of a stabilizing agent,[10,11,16] and detailed discussion on this aspect is beyond the scope of this study.

Surface area development

While SEM imaging provides direct visual evidence of the particle size, it can not quantify the size with high statistical confidence due to limited number of iron particles analyzed. An indirect but more reliable approach to gauge the particle size is to measure the surface area. It is also much more efficient and cost-effective relative to microscopic analysis. In addition, abundant BET surface area data of ZVI materials are available in the literature for comparison.[2,33–35]

In this work, BET specific surface areas (a_s) were measured on iron samples after various milling times. Fig. 4a shows the measured a_s values as a function of the milling time. The feed material, BASF micron-sized iron, has an a_s of 0.41 $m^2\ g^{-1}$. After 8 hours of milling, specific surface area of iron increases to 39 $m^2\ g^{-1}$, corresponding to an over 95 times increase. The plot of specific surface area *versus* time can be best-fit by a linear trendline ($R^2 = 0.978$) with a slope of approximately 4.15 $m^2\ g^{-1}\ h^{-1}$. Repeated milling experiments using the same source of feed iron show that the a_s measured at a given time do not differ significantly among different milling batches, and as a general benchmark, a_s is over 25 $m^2\ g^{-1}$after 6 hours of milling.

Equivalent sphere diameter

Assuming a spherical geometry, specific surface area (a_s) of a particle can be calculated from the particle diameter (D):

$$\text{Specific Surface Area} = a_s = \frac{\text{Surface}}{\text{Mass}} = \frac{\pi D^2}{\frac{1}{6}\pi D^3 \rho} = \frac{6}{\rho D} \quad (2)$$

where ρ represents the density of metallic iron (7800 kg m^{-3}). Given the specific surface area, an equivalent sphere diameter (D) of iron particles can be calculated by the following equations:

$$D = \frac{6}{\rho a_s} \quad (3)$$

D of the feed iron is calculated to be ~1900 nm using eqn (3), in good agreement with the information provided by the supplier (d_{50}= 2 μm). Note that in eqn (2) and (3) it is assumed that all particles are of spherical shape and equal size. For actual samples, especially for milled particles, particle shapes deviate from perfect sphere, and particle sizes are poly-dispersed and the

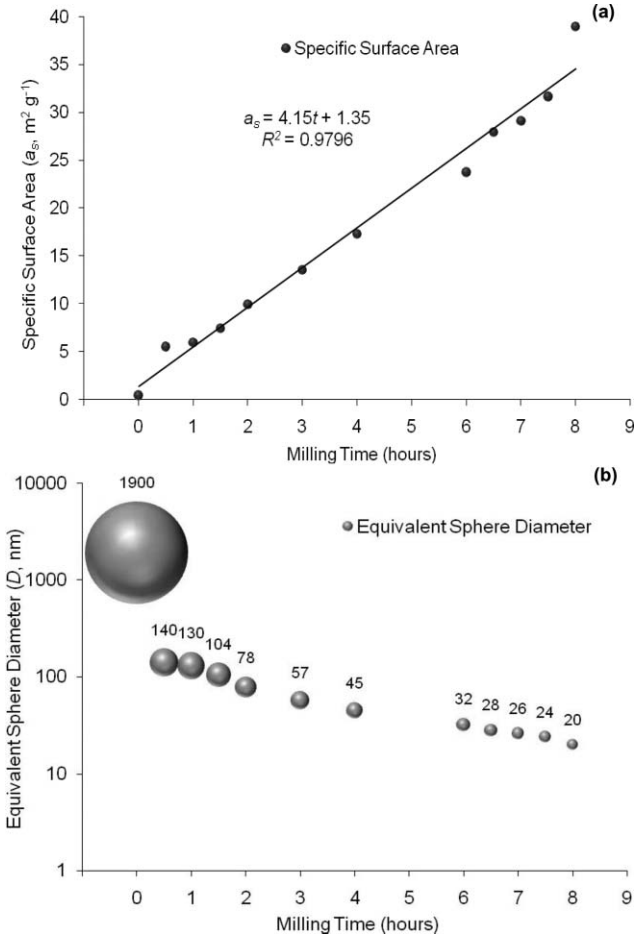

Fig. 4 (a) Specific surface area (a_s) of iron as a function of milling time. (b) Trend of calculated equivalent sphere diameter (D) at different milling times.

distribution often skews towards smaller ones. Thus, D values represent crude estimates of the particle sizes only. Still, the easy of calculating D and the tangible physical meaning it embodies make it a convenient parameter to assess the progressive size reduction achieved in the milling process. Fig. 4b displays the trend of D at different milling times. At 8 hours, D is approximately 20 nm, which is in good agreement with the SEM imaging illustrated in Fig. 3c and d. With independent evidence provided by the two vastly different approaches, the effectiveness of the ball milling method to produce nano-scale ZVI material is convincingly demonstrated.

From a reactivity point of view, surface area is actually a more important parameter than the particle size. Contaminant degradation reactions are generally regarded as mediated by ZVI surface, and the reaction rates are dependent on the ZVI surface area available. Kinetics studies on a number of chlorinated contaminants suggest that the enhanced reactivity of non-modified nZVI stems primarily from the increase in surface area.[13,15,36] Reaction kinetics have been conveniently expressed as a pseudo-first-order reaction normalized to the surface area:[2] where C is the contaminant concentration in

$$\frac{dC}{dt} = -K_{SA} a_s \rho C \quad (4)$$

Table 1 Surface areas and calculated size (D) of selected iron materials

Iron	Surface Area, a_s/m^2 g^{-1}	Size information (D)	Supplier/ Reference
Iron powder	0.0015	0.425–2 mm	Alfa Aesar/31
Electrolytic iron	0.16	100 mesh	Fisher/33
Micron iron powder	0.30	<10 μm	Sigma-Aldrich
nZVI (H_2 reduction)	23	40–60 nm	Toda/15
(nZVI^B)[a]	25~35	10–100 nm	12–16
Micro iron (feed, 0 hour, d_{50}= 2 μm)	0.41	1900 nm[b]	BASF/This work
0.5 hour-milling	5.5	140 nm[b]	This work
2 hour-milling	9.9	79 nm[b]	This work
4 hour-milling	17	44 nm[b]	This work
6 hour-milling	24	32 nm[b]	This work
8 hour-milling	39	20 nm[b]	This work

[a] nZVI^B refers to nZVI prepared by the borohydride method. [b] Calculated by eqn (3).

the solution (mg L^{-1}), K_{SA} is the surface-area-normalized rate constant (L h^{-1} m^{-2}), a_s is the specific surface area of iron particle (m^2 g^{-1}), ρ is the mass concentration of ZVI (g L^{-1}), and t is reaction time (h). Specific surface areas (a_s) of ZVI materials produced by different methods and from different sources are listed in Table 1. With 8 hours of milling, the a_s is increased by nearly 2 orders of magnitude relative to the feed iron, and a large enhancement in reactivity is thus anticipated. The surface area data will be used in a later section to compare the reactivity of nZVI in terms of dechlorination reaction rates with that of other ZVI materials.

XPS characterization

Fig. 5a presents a XPS wide-scan of the iron samples to reveal their surface chemical compositions. The photoelectron peaks indicate that the surfaces of the feed iron and its milled product are comprised of iron and oxygen, as well as small amounts of adventitious carbon. Essentially the same results were obtained in the previous studies on the borohydride-reduced nZVI (hereafter termed nZVI^B), which indicate oxygen and iron as the two principle elements on the surface.[37] A noticeable difference between the milled sample and the nZVI^B is the absence of boron from the milled iron.

High-resolution XPS (HR-XPS) scans (Fig. 5b and c) provide additional details on the surface chemical composition and the chemical states of iron and oxygen on the surface. Fig 5b shows the scan at Fe 2p region. For the three samples examined, the prevailing state of iron near the surface region is oxidized iron, Fe(III), represented by the photoelectron peaks at ~711 and ~725 eV based on the binding energies of $2p_{3/2}$ and $2p_{1/2}$ of Fe(III). Relatively small peaks in comparison to the strong Fe(III) peaks were detected at 706.5 eV, which are assigned to Fe(0) $2p_{3/2}$. For the milled nZVI, a small shoulder with binding energy at *ca.* 709 eV related to Fe(II) species is also detected, which implies Fe(II) oxide or mixed valent oxides (*e.g.* Fe_3O_4) are present at the surface as products or intermediate species of Fe(0) oxidation. Based on these results, it can be concluded that the iron species at the near-surface region of these three samples had been extensively oxidized, with only a small fraction of Fe(0) remaining.

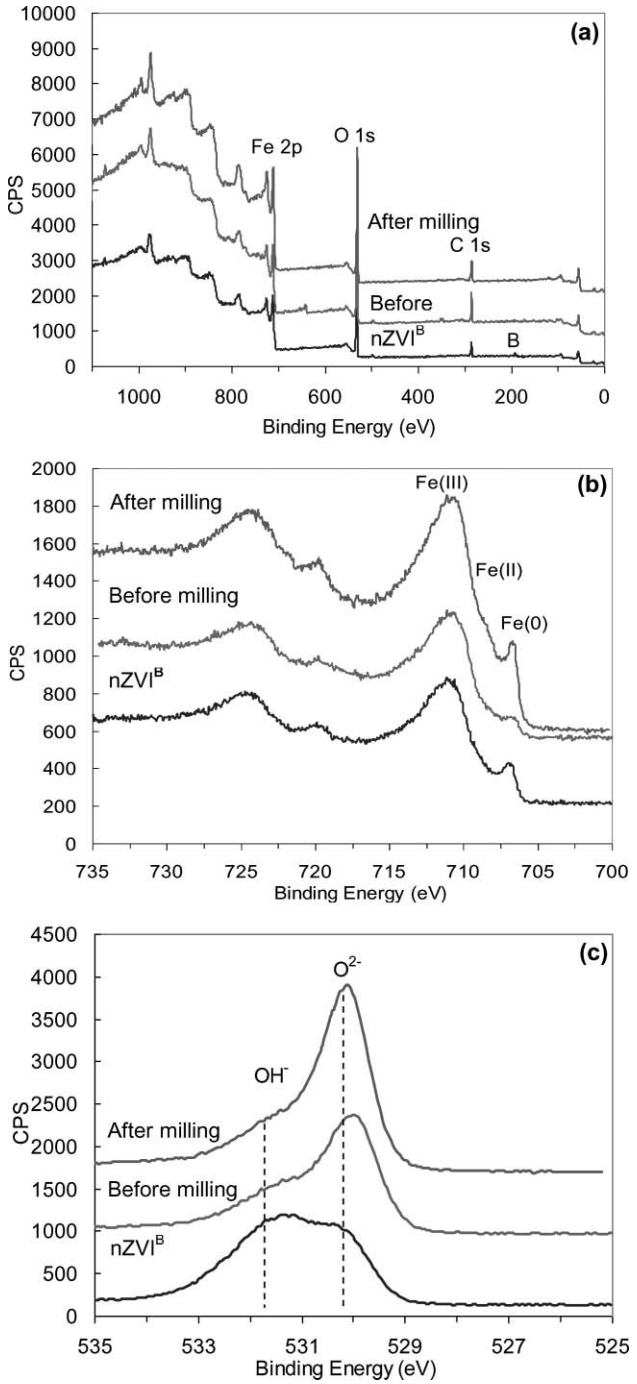

Fig. 5 XPS analysis of iron powders before and after 8 hours of milling *versus* the chemically synthesized nZVI (nZVI^{B}). (a) XPS wide scan. (b) Detail scan at Fe 2p region. (c) Detail scan at O 1 s region.

As shown in Fig. 5b, the Fe(0) peak from the feed iron is barely visible. By comparing the peak area of Fe(0) to other iron species, it is evident that the milled nZVI has a significantly greater proportion of Fe(0) in the surface region than the feed iron. The effect arises from breaking down of the micron-sized feed particles into much smaller fragments during the milling process, exposing the interior metallic iron in the precursor particle to the newly-formed surfaces, as well as the abrasive effect of the mechanical impacts that caused the surface oxide layer to be highly defective and more metallic iron being exposed.

Fig. 5c delineates the XPS scan at the O1*s* region to reveal the chemical structure of the surface oxides. Surface oxide composition of iron materials is known to depend on the fabrication methods and to a certain degree on the environmental conditions during the synthesis. Two peaks are observed at *ca.* 530 eV and 531.6 eV, representing the oxygen in the form of O^{2-} and OH^{-}, respectively. The spectrum of the milled nZVI is largely similar to that of the feed iron, both having a dominant O^{2-} peak and a very weak OH^{-} peak, indicating the nature of the surface oxide is not altered by milling. A slight increase in the O^{2-} peak in the milled ZVI may result from oxidation of the exposed metallic iron during the milling step. On the other hand, the OH^{-} peak is much more prominent on the borohydride-reduced nZVI (nZVI^{B}). The relative abundance of OH^{-} reflects the oxide phase in nZVI^{B} originates from aqueous corrosion of Fe(0) and hydroxide precipitation, a fact that is consistent with the synthesis environment of nZVI^{B}. Based on the XPS O1*s* result, the stoichiometric composition of the oxide in nZVI^{B} can be described as FeOOH.[31,37] The milled iron, in contrast, barely contains the hydroxide phase, and taking into account the Fe 2*p* XPS signals, it can be inferred that the outer layer of the milled nZVI comprises mainly of Fe_2O_3 with small amounts of FeO or Fe_3O_4. The presence of these oxide phases has been reported in other types of nZVI produced *via* physical methods, *e.g.*, sputtering and nucleation of metallic vapor generate iron nanoparticles whose oxide shell consists of either γ-Fe_2O_3 or Fe_3O_4.[38]

XRD analysis

Fig. 6 presents X-ray diffraction (XRD) results of the feed and milled iron. The feed iron shows only the presence of sharp α-Fe peaks, thus, the material is comprised essentially of pure crystalline α-Fe. Broadening of these two α-Fe peaks after milling indicates the reduction in crystal grain size as a result of particle fragmentation. A few new peaks, albeit with much weaker intensities, emerge after milling. The new peaks are characteristic of magnetite (Fe_3O_4), or maghemite (γ-Fe_2O_3),

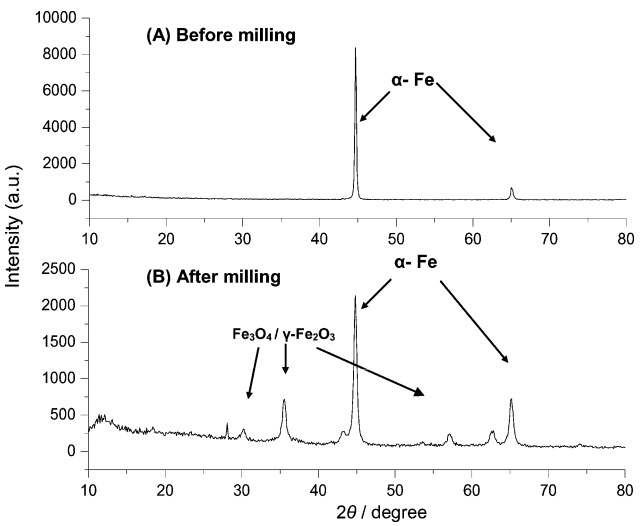

Fig. 6 XRD patterns of iron powders before and after 8 hours of milling.

which are in accordance with our XPS results. In addition, α-Fe and iron oxide had been detected with the nZVI^{B}.[31]

Reactions with water

In an aqueous environment, ZVI readily reacts with water or dissolved oxygen (eqn (5) and (6)).

$$Fe^0\ (s) + 2\ H_2O \rightarrow Fe^{2+} + H_2\ (g) + 2\ OH^- \quad (5)$$

$$2\ Fe^0\ (s) + 2\ H_2O + O_2 \rightarrow 2\ Fe^{2+} + 4\ OH^- \quad (6)$$

Since water molecules are ubiquitous in the aqueous environment and contaminants typically exist at trace levels, the above reactions take place to a considerable extent in parallel to the reactions between ZVI and contaminants. Hydrogen gas evolution, increase in solution pH and concurrent decrease in the oxidation-reduction potential (Eh) are therefore anticipated after sufficient ZVI is added to water. Due to the large surface area of nanoparticles, more intense reactions between nZVI and water are also expected. In DI water with small amounts (<0.01 g L^{-1}) of nZVI^{B}, an instant pH surge to 9 and E_h decrease to –400 mV have been reported.[31] For field applications of nZVI, solution pH and E_h changes have often been used as the key water chemistry parameters for quick assessments of nZVI reactivity.[12,39]

In this work, the aqueous reactivity of five iron materials, namely, micro iron (the feed), milled irons (milling time 0.5, 4, and 8 hours) and chemically synthesized nZVI (nZVI^{B}) were studied at the same iron loading of 0.5 g L^{-1}. Results suggest all of these five irons increased the solution pH from 6 to *ca.* 9 in less than 10 minutes (data not shown). The accompanying solution E_h decreases using these five materials are also observed (Fig. 7). In spite of the identical initial conditions, the solution E_h evolved differently. In the solution containing the micro iron (feed), a gradual decrease of E_h from +400 mV to +211 mV was recorded in 30 minutes. In the solutions with the milled irons, E_h declined at much steeper rates and the final values after 30 minutes were around –379 mV or lower. It is evident that iron processed for a longer milling time gives a more rapidly declining E_h trend, indicative of a higher aqueous corrosion rate resultant from the increase in iron surface area. The trend of the chemically synthesized nZVI (nZVI^{B}) falls in an intermediate region defined by iron milled for 0.5 and 4 hours. In short, the finished product (8 hours of milling) demonstrated a higher reactivity than the nZVI^{B} at the same mass loading.

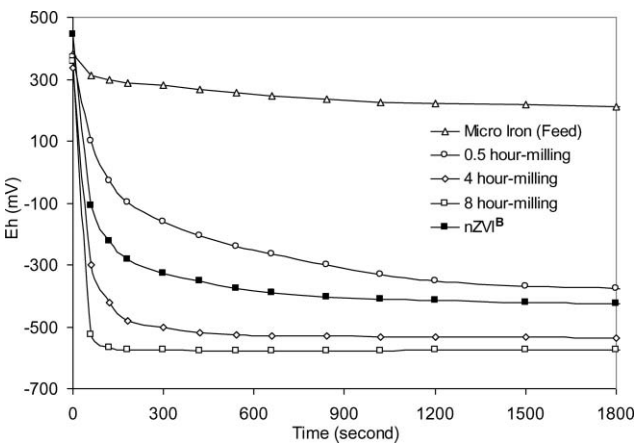

Fig. 7 Evolution of solution E_h in distilled water with five ZVI materials (mass loading 0.5 g L^{-1}).

Reactions with chlorinated aliphatic hydrocarbons

So far, nZVI has been used primarily in the remediation of sites contaminated with chlorinated organic compounds.[12] The ability to degrade chlorinated compounds is thus a vital indicator of iron reactivity. In this work, seven chlorinated aliphatic hydrocarbons were selected as model contaminants, namely, 1,1-DCA ($CHCl_2CH_3$), 1,1,1-TCA (CCl_3CH_3), CT (CCl_4), 1,2-DCA (CH_2ClCH_2Cl), TCE (C_2HCl_3), PCE (C_2Cl_4) and 1,1,2,2-TeCA ($CHCl_2CHCl_2$), with consideration that these compounds are among the most frequently detected contaminants in groundwater.[40]

Fig. 8 shows gas chromatograms of mixtures of the seven compounds before and after reactions with the micro iron (feed), irons milled for 4 and 8 hours, and nZVI^{B}. Identical mass of iron materials (10 g L^{-1}) and the same initial concentration of each compound (25 mg L^{-1}) were used. A control experiment with no ZVI is also shown. All four iron materials demonstrate excellent efficiency (>99%) for the removal of 1,1,1-TCA, CT, 1,1,2,2-TeCA. They exhibit different reactivity towards 1,1-DCA, 1,2-DCA, TCE and PCE. For the micro iron, less than 30% removal of TCE and PCE were achieved, while 1,1-DCA and 1,2-DCA essentially remained unaffected. nZVI^{B} removes nearly 50 to 73% TCE and PCE and approximately 30% of 1,1-DCA and 1,2-DCA. For iron milled for 4 hours, all TCE and PCE were degraded while only 13–23% of the two DCAs

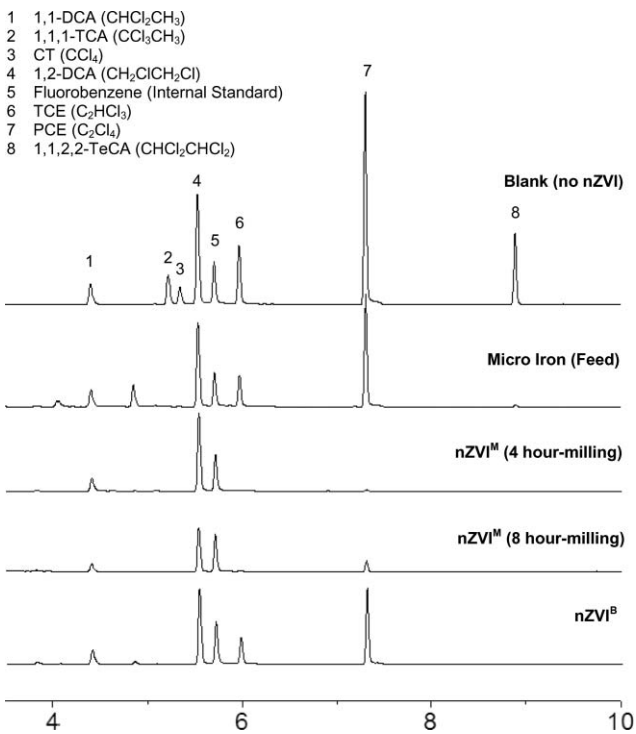

Fig. 8 Gas chromatograms of products from reaction of various nZVI materials with seven chlorinated hydrocarbons (ZVI mass loading 10 g L^{-1}, contaminant initial concentration 25 mg L^{-1} each, reaction time 48 hours).

Table 2 Treatment efficiency of seven chlorinated aliphatic compounds using four ZVI materials

	Micro iron (feed)[a]	nZVI^{M} (4 hour-milling)[a]	nZVI^{M} (8 hour-milling)[a]	(nZVI^{B})[a]
1,1-DCA[b]	< 1.0%	23.2%	59.7%	29.8%
1,2-DCA[b]	< 1.0%	13.2%	53.7%	30.0%
TCE[b]	25.1%	99.5%	99.0%	50.1%
PCE[b]	28.6%	99.4%	94.1%	73.3%
1,1,2,2-TeCA[b]				
1,1,1-TCA[b]		>99.0%		
CT[b]				

[a] ZVI mass loading 10 g L^{-1}, reaction time 48 hours. [b] Contaminant initial concentration 25 mg L^{-1} each.

were removed. The best performance came from the iron milled for 8 hours. It reduced over 90% for TCE and PCE and over 50% of DCAs. A summary of the removal efficiency is included in Table 2. It is apparent that the reactivity of the iron materials for dechlorination increases with the milling time, that is, 8 hours milling > 4 hours milling > feed (micro iron).

Based on the reactions with water and with the seven chlorinated organic compounds, it can be concluded that the milled nZVI is more reactive than the nZVI^{B}. The milling process improves the reductive reactivity of iron as a result of the enlarged surface area. The nZVI milled for 8 hours has an a_s of 39 m^2 g^{-1}, larger than the synthesized nZVI^{B} (*ca.* 30 m^2 g^{-1}). Another potential reason is the fresher surface with more ZVI atoms on the milled iron. The Fe^0 peak height and its integrated area from XPS scans suggest that there are more ZVI atoms on the surface of milled nZVI. The increased availability of fresh ZVI atoms in the near surface region enhances and accelerates the oxidation of iron. This may explain the better results obtained with the milled nZVI.

Waste assessment

For every kilogram of nZVI manufactured, the only material used in precision milling is nearly the same amount of micro iron powder, and no byproduct is generated in the entire process. In comparison, conventional preparation methods, namely, the borohydride reduction and iron pentacarbonyl decomposition, use 3–6 times more feed materials, which include toxic and hazardous chemicals, such as $Fe(CO)_5$ and $NaBH_4$. Furthermore, these chemical methods inevitably lead to the generation of significant volumes of waste streams entailing additional costs for their proper treatment and disposal. Evolution of highly flammable and toxic gases such as H_2 and CO in these processes raises safety concerns in large-scale production. In short, the milling method presented in this work is a truly green technology.

Conclusion

It is demonstrated through size and surface area characterizations that the precision ball-milling process described in this work offers an effective method to produce nano-scale ZVI particles with particle size and surface area readily controllable by the milling time. With 8 hours of milling, the particles produced are of an equivalent sphere diameter of 20 nm and a surface area of 39 m^2 g^{-1}; both parameters surpass those of nZVI synthesized with the sodium borohydride method. Reactions towards water and seven common chlorinated contaminants confirm the milled nZVI (8 hour-milling) has superior chemical reactivity over the chemically made nZVI. The milling method presented here is completely scalable for large quantity production of nZVI,[29,30] delivers nearly 100% yield of iron, uses no hazardous materials and produces no waste in the production process. It offers an attractive route to green manufacturing of iron nanoparticles and brings the nZVI technology one step closer to large-scale *in situ* remediation.

References

1 R. W. Gillham and S. F. Ohannesin, *Ground Water*, 1994, **32**, 958–967.
2 T. L. Johnson, M. M. Scherer and P. G. Tratnyek, *Environ. Sci. Technol.*, 1996, **30**, 2634–2640.
3 T. E. Shokes and G. Moller, *Environ. Sci. Technol.*, 1999, **33**, 282–287.
4 S. R. Kanel, B. Manning, L. Charlet and H. Choi, *Environ. Sci. Technol.*, 2005, **39**, 1291–1298.
5 M. J. Alowitz and M. M. Scherer, *Environ. Sci. Technol.*, 2002, **36**, 299–306.
6 C. P. Huang, H. W. Wang and P. C. Chiu, *Water Res.*, 1998, **32**, 2257–2264.
7 S. Nam and P. G. Tratnyek, *Water Res.*, 2000, **34**, 1837–1845.
8 K. Ritter, M. S. Odziemkowski, R. Simpgraga, R. W. Gillham and D. E. Irish, *J. Contam. Hydrol.*, 2003, **65**, 121–136.
9 L. M. Ma and W. X. Zhang, *Environ. Sci. Technol.*, 2008, **42**, 5384–5389.
10 T. Phenrat, N. Saleh, K. Sirk, H. J. Kim, R. D. Tilton and G. V. Lowry, *J. Nanopart. Res.*, 2008, **10**, 795–814.
11 B. Schrick, B. W. Hydutsky, J. L. Blough and T. E. Mallouk, *Chem. Mater.*, 2004, **16**, 2187–2193.
12 D. W. Elliott and W. X. Zhang, *Environ. Sci. Technol.*, 2001, **35**, 4922–4926.
13 H. Song and E. R. Carraway, *Environ. Sci. Technol.*, 2005, **39**, 6237–6245.
14 C. Lee, J. Y. Kim, W. Il Lee, K. L. Nelson, J. Yoon and D. L. Sedlak, *Environ. Sci. Technol.*, 2008, **42**, 4927–4933.
15 Y. Q. Liu, S. A. Majetich, R. D. Tilton, D. S. Sholl and G. V. Lowry, *Environ. Sci. Technol.*, 2005, **39**, 1338–1345.
16 C. B. Wang and W. X. Zhang, *Environ. Sci. Technol.*, 1997, **31**, 2154–2156.
17 C. G. Granqvist and R. A. Buhrman, *J. Appl. Phys.*, 1976, **47**, 2200–2219.
18 H. Hahn, *Nanostruct. Mater.*, 1997, **9**, 3–12.
19 K. S. Suslick, S. B. Choe, A. A. Cichowlas and M. W. Grinstaff, *Nature*, 1991, **353**, 414–416.
20 X. Cao, Y. Koltypin, G. Kataby, R. Prozorov and A. Gedanken, *J. Mater. Res.*, 1995, **10**, 2952–2957.
21 J. L. Cain and D. E. Nikles, *J. Appl. Phys.*, 1996, **79**, 4860–4862.
22 P. Majewski and B. Thierry, *Crit. Rev. Solid State Mater. Sci.*, 2007, **32**, 203–215.
23 I. Capek, *Adv. Colloid Interface Sci.*, 2004, **110**, 49–74.
24 R. Choukroun, D. de Caro, S. Mateo, C. Amiens, B. Chaudret, E. Snoeck and M. Respaud, *New J. Chem.*, 1998, **22**, 1295–1299.
25 E. Bermejo, T. Becue, C. Lacour and M. Quarton, *Powder Technol.*, 1997, **94**, 29–34.
26 A. Dierstein, H. Natter, F. Meyer, H. O. Stephan, C. Kropf and R. Hempelmann, *Scr. Mater.*, 2001, **44**, 2209–2212.
27 C. Suryanarayana, *Prog. Mater. Sci.*, 2001, **46**, 1–184.
28 L. B. Kong, T. S. Zhang, J. Ma and F. Boey, *Prog. Mater. Sci.*, 2008, **53**, 207–322.
29 NETZSCH Fine Particle Technology | Leading global manufacturer of advanced process technology, http://grinding.netzschusa.com/, accessed on April 9, 2009.
30 NETZSCH Fine Particle Technology, http://grinding.netzschusa.com/products/wet_grinding/Lab_Equipment/Labstar/Labstar.html, accessed on April 9, 2009.

31 Y. P. Sun, X. Q. Li, J. S. Cao, W. X. Zhang and H. P. Wang, *Adv. Colloid Interface Sci.*, 2006, **120**, 47–56.
32 H. L. Lien and W. X. Zhang, *Colloids Surf., A*, 2001, **191**, 97–105.
33 W. A. Arnold and A. L. Roberts, *Environ. Sci. Technol.*, 2000, **34**, 1794–1805.
34 J. P. Fennelly and A. L. Roberts, *Environ. Sci. Technol.*, 1998, **32**, 1980–1988.
35 A. L. Roberts, L. A. Totten, W. A. Arnold, D. R. Burris and T. J. Campbell, *Environ. Sci. Technol.*, 1996, **30**, 2654–2659.
36 J. T. Nurmi, P. G. Tratnyek, V. Sarathy, D. R. Baer, J. E. Amonette, K. Pecher, C. M. Wang, J. C. Linehan, D. W. Matson, R. L. Penn and M. D. Driessen, *Environ. Sci. Technol.*, 2005, **39**, 1221–1230.
37 X. Q. Li and W. X. Zhang, *J. Phys. Chem. C*, 2007, **111**, 6939–6946.
38 L. T. Kuhn, A. Bojesen, L. Timmermann, M. M. Nielsen and S. Morup, *J. Phys.: Condens. Matter*, 2002, **14**, 13551–13567.
39 X. Q. Li, D. W. Elliott and W. X. Zhang, *Crit. Rev. Solid State Mater. Sci.*, 2006, **31**, 111–122.
40 2007 CERCLA Priority List of Hazardous Substances (available from http://www.atsdr.cdc.gov/cercla/05list.html).

